Pergamon

PII S1359-6454(96)00137-1

Acta mater. Vol. 45, No. 1, pp. 245–255, 1997

Published by Elsevier Science Ltd

1359-6454/97 $17.00 + 0.00

COMPUTER SIMULATION OF THE KINETICS OF ORDER–DISORDER AND PHASE SEPARATION DURING PRECIPITATION OF δ' (Al_3Li) IN Al–Li ALLOYS

R. PODURI and L.-Q. CHEN

Department of Materials Science and Engineering, The Pennsylvania State University, University Park, PA 16802, U.S.A.

(Received 25 October 1996; accepted 9 April 1996)

Abstract—A computer simulation study has been performed of the reaction paths for the precipitation of δ' (Al_3Li) ordered particles from a disordered matrix (α) in Al–Li alloys, using microscopic Langévin diffusion equations. It is found that the precipitation of δ' occurs either by a congruent ordering process followed by decomposition, or by a non-classical nucleation mechanism which requires critical fluctuations of both composition and order parameter, except in a narrow range of compositions near the equilibrium phase boundary of the disordered phase, where classical nucleation theory seems to be applicable. Composition and order parameter profiles across a critical nucleus were obtained for different compositions in the nucleation and growth regime, and compared with those obtained from the continuum non-classical nucleation theory. Possible origins for the discrepancies in the precipitation mechanism, obtained from different theoretical and experimental studies, are suggested. *Copyright © 1996 Acta Metallurgica Inc.*

1. INTRODUCTION

The precipitation process of metastable δ' (Al_3Li) ordered phase particles from a disordered Al–Li solid solution, α, has drawn considerable interest in recent years, due to the potential applications of precipitation strengthened lightweight materials in the aerospace industry. However, despite extensive research on this system, there exist controversies in the literature regarding the underlying kinetic mechanisms for this precipitation process.

Based on a thermodynamic stability analysis, Khachaturyan *et al.* [1] proposed that when the Li composition, c, is above c_- [see Fig. 1(b)], the disordered phase undergoes a congruent ordering process, i.e. an ordering reaction without any compositional changes, followed by spinodal decomposition of the congruently ordered single phase into Li-rich and Li-lean ordered regions, with the low-Li regions spontaneously becoming disordered after their compositions reach the instability limit, c_+, for the ordered phase. When c was between c_- and c', a congruent ordering reaction, taking place by classical nucleation and growth, was proposed, again to be followed by spinodal decomposition. And when c was below c' it was proposed that the precipitation process follows the classical nucleation and growth mechanism.

While some of the experimental works [2–5] claimed to have confirmed the existence of congruent ordering of the Al–Li system as predicted by thermodynamic stability analysis, other observations can only be explained by the classical nucleation growth mechanism [6, 7]. In other related alloy systems, it has been found [8–11] that as the initial average composition of the disordered phase increases towards c_-, precipitation of the ordered compound takes place by a non-classical nucleation mechanism, with the critical nuclei having compositions that are significantly different from that of the equilibrium ordered phase.

Recently, we extended the continuum non-classical nucleation theory of Cahn and Hilliard for isostructural decomposition to the case of precipitation of ordered intermetallics from a disordered matrix [12]. It was shown that it is only when the matrix composition is near the phase boundary of the disordered phase, that the composition and order parameter values inside the nucleus are close to those of the equilibrium ordered phase, and that the critical profiles become increasingly diffuse as the ordering instability line is approached. In contrast to thermodynamic stability analysis, which predicted a region of congruent nucleation and growth, it is found that the critical nucleus consists of both composition and order parameter fluctuations through the entire composition range, from the disordered phase boundary to the ordering instability line.

The continuum non-classical nucleation theory is purely a thermodynamic analysis of the saddle points

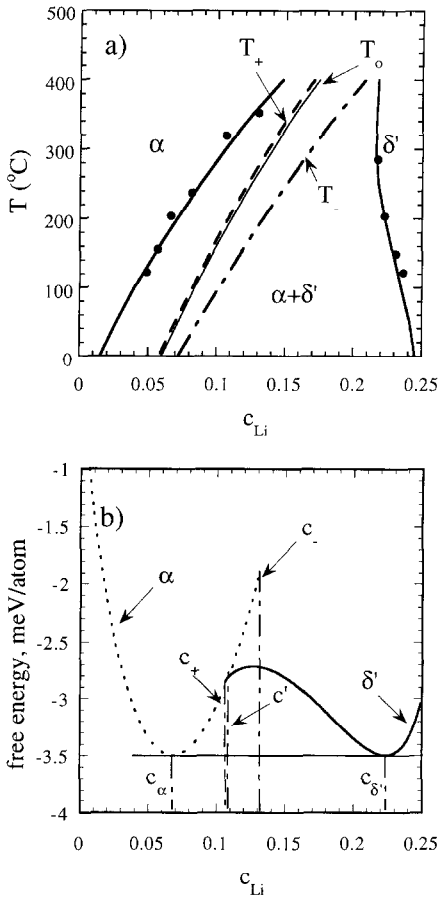

Fig. 1. (a) Computed Al–Li phase diagram and (b) free energy–composition curves for $T = 465$ K.

on the free energy hypersurface in the coordinates of composition and order parameter profiles, i.e. the properties of a critical nucleus. Although the thermodynamic stability analysis of Khachaturyan utilized the kinetic argument that ordering, which requires atomic diffusion of the order of atomic lattice spacing, occurs much faster than phase separation, which requires a diffusion distance of the order of the precipitate size, it is again mainly a thermodynamic analysis. In order to predict the actual kinetics which take place during the precipitation of order intermetallics from a disordered matrix and the relative growth rates of compositional heterogeneities and long-range order, a kinetic theory must be employed. In this paper, the microscopic diffusion equations of Khachaturyan [13], in combination with a thermal noise term, will be applied to the particular case of the precipitation of δ' (Al_3Li) ordered particles from a disordered f.c.c. matrix. The main purpose is to obtain a fundamental understanding of the precipitation process in different compositional regimes within the two-phase field, and to suggest possible reasons for the differences obtained in different experimental and theoretical studies on this system.

2. THE MICROSCOPIC DIFFUSION THEORY

In the microscopic diffusion theory, the atomic configuration and the morphologies of an alloy are described by a single-site occupation probability function, $P(\mathbf{Ar}, t)$, which is the probability that a given lattice site, $\mathbf{r}$, is occupied by a given atom of type A (e.g. Li in Al Li alloys), at a given time t. The rates of change of these probabilities are then described by the Onsager-type diffusion equations as being linearly proportional to the thermodynamic driving force [13]:

$$\frac{dP(\mathbf{Ar}, t)}{dt} = \frac{c_A(1 - c_A)}{k_B T} \sum_{\mathbf{r}'} L(\mathbf{r} - \mathbf{r}') \frac{\delta F}{\delta P(\mathbf{Ar}', t)} \quad (1)$$

where the summation is carried out over all N crystal lattice sites of a system, $L(\mathbf{r} - \mathbf{r}')$ is the proportionality constant which is related to the probability of an elementary diffusion jump from site $\mathbf{r}$ to $\mathbf{r}'$, per unit of time, T is temperature, k_B is the Boltzmann constant, c_A is the atomic fraction of the A component, and F is the total free energy of the system, which is a functional of the single-site occupation probability function.

Kinetic equation (1) is deterministic and hence cannot describe processes that require thermal fluctuations, such as nucleation. Therefore, in order to be able to study the nucleation and growth and spinodal processes on the same footing, we introduce a random noise term, $\xi(\mathbf{r}, t)$, to the kinetic equation (1) to simulate the thermal fluctuations:

$$\frac{dP(\mathbf{Ar}, t)}{dt} = \frac{c_A(1 - c_A)}{k_B T} \sum_{\mathbf{r}'} L(\mathbf{r} - \mathbf{r}') \times \frac{\delta F}{\delta P(\mathbf{Ar}', t)} + \xi(\mathbf{r}, t) \quad (2)$$

where $\xi(\mathbf{r}, t)$ is assumed to be Gaussian-distributed with average zero, and uncorrelated with respect to both space and time, i.e. it obeys the so-called fluctuation dissipation theory [14, 15]:

$$\langle \xi(\mathbf{r}, t) \rangle = 0$$

$$\langle \xi(\mathbf{r}, t) \xi(\mathbf{r}', t') \rangle = -2 k_B T L(\mathbf{r} - \mathbf{r}') \delta(t - t') \delta(\mathbf{r} - \mathbf{r}') \quad (3)$$

where $\langle \ldots \rangle$ denotes an averaging, $\langle \xi(\mathbf{r}, t) \rangle$ is the average value of the noise over space and time, $\langle \xi(\mathbf{r}, t) \xi(\mathbf{r}', t') \rangle$ is the correlation and δ is the Kronecker delta function. The noise term is similar to that introduced by Cook to the Cahn–Hilliard equation [16]. With the noise term, equation (2) becomes stochastic and is, in fact, the microscopic version of the continuum Langévin equation [17].

The corresponding growth rates in the amplitudes of composition modulations, $\tilde{P}(\mathbf{k}, t)$, at a given wave

vector, $\mathbf{k}$, can be easily obtained by taking the Fourier transform of equation (2), i.e.

$$\frac{d\tilde{P}(\mathbf{AK}, t)}{dt} = \frac{c_A(1-c_A)}{k_B T}\tilde{L}(\mathbf{k}) \times \left\{\frac{\delta F}{\delta P(\mathbf{Ar}, t)}\right\}_{\mathbf{k}} + \xi(\mathbf{k}, t) \quad (4)$$

where $\tilde{P}(\mathbf{k}, t)$, $\tilde{L}(\mathbf{k})$, $[\delta F/\delta P(\mathbf{Ar}, t)]_{\mathbf{k}}$, and $\xi(\mathbf{k}, t)$ are the Fourier transforms of $P(\mathbf{Ar}, t)$, $L(\mathbf{r})$, $[\delta F/\delta P(\mathbf{Ar}, t)]$, and $\xi(\mathbf{r}, t)$, respectively.

3. COMPUTER SIMULATION

3.1. Application to an f.c.c. lattice

In the mean-field approximation, the total free energy of a system is given by

$$F = \frac{1}{2}\sum_{\mathbf{r}}\sum_{\mathbf{r}'} W(\mathbf{r}-\mathbf{r}')P(\mathbf{r})P(\mathbf{r}') + k_B T \sum_{\mathbf{r}} [P(\mathbf{r})\ln P(\mathbf{r}) + (1-P(\mathbf{r}))\ln(1-P(\mathbf{r}))] \quad (5)$$

where $W(\mathbf{r}-\mathbf{r}')$ is the effective interchange interaction energy given as the sum of the A–A and B–B pairwise interaction energies, minus twice the A–B pairwise interaction energy:

$$W(\mathbf{r}-\mathbf{r}') = W_{AA}(\mathbf{r}-\mathbf{r}') + W_{BB}(\mathbf{r}-\mathbf{r}') - 2W_{AB}(\mathbf{r}-\mathbf{r}'). \quad (6)$$

Using equations (5) and (4), we have

$$\frac{d\tilde{P}(\mathbf{k}, t)}{dt} = \frac{c_A(1-c_A)}{k_B T}\tilde{L}(\mathbf{k})\left\{\tilde{V}(\mathbf{k})\tilde{P}(\mathbf{k}, t) + k_B T\left[\ln\left(\frac{P(\mathbf{Ar}, t)}{1-P(\mathbf{Ar}, t)}\right)\right]_{\mathbf{k}}\right\} + \xi(\mathbf{k}, t) \quad (7)$$

in which $\tilde{V}(\mathbf{k})$ is the Fourier transform of $W(\mathbf{r})$, and for an f.c.c. lattice, is given by

$$\tilde{V}(\mathbf{k}) = 4W_1(\cos\pi h\cdot\cos\pi k + \cos\pi h\cdot\cos\pi l + \cos\pi k\cdot\cos\pi l) + 2W_2(\cos 2\pi h + \cos 2\pi k + \cos 2\pi l) + \cdots \quad (8)$$

where W_1 and W_2 are the first-nearest and second-nearest neighbor effective interchange interaction energies, respectively, and h, k and l are integers, related to the reciprocal lattice through

$$\mathbf{k} = (k_x, k_y, k_z) = 2\pi(h\mathbf{a}_1^* + k\mathbf{a}_2^* + l\mathbf{a}_3^*)$$

with $\mathbf{a}_1^*$, $\mathbf{a}_2^*$, and $\mathbf{a}_3^*$ being the unit reciprocal lattice vectors of the f.c.c. lattice along the [100], [010], and [001] directions, respectively, and $|\mathbf{a}_1^*| = |\mathbf{a}_2^*| = |\mathbf{a}_3^*| = 1/a_0$ (a_0 is the lattice parameter of the f.c.c. lattice).

By assuming atomic jumps between nearest neighbor sites only and using the condition that the total number of atoms in the system is conserved, for an f.c.c. lattice, we can write [13]

$$\tilde{L}(\mathbf{k}) = -4L_1[3 - \cos\pi h\cdot\cos\pi k - \cos\pi k\cdot\cos\pi l - \cos\pi l\cdot\cos\pi h] \quad (9)$$

where L_1 is proportional to the jump probability between nearest-neighbor sites per unit of time.

3.2. Two-dimensional (2-D) approximation of a 3-D problem

Although it is straightforward and desirable to perform 3-D simulations using the microscopic diffusion equations outlined above, a 2-D simulation is much less computationally intensive, and the analysis and visualization of the atomic configuration and multiphase morphologies are much easier. Consequently, all the results reported in this paper were obtained using 2-D projections of a 3-D system. A test simulation using a 3-D system yields essentially the same results on the precipitation mechanism that we are interested in. It is equivalent to assuming that the occupation probabilities do not depend on the coordinate z along the [001] axis. The formulation of the kinetic equations on a 2-D projection of a 3-D f.c.c. lattice presented below was suggested by Khachaturyan [18a].

The 2-D projection of an f.c.c. lattice along the [001] direction is a square lattice whose lattice parameter is half that of the f.c.c. lattice. Therefore, a lattice vector $\mathbf{r}$ in the 2-D square lattice can be written as

$$\mathbf{r} = x'\mathbf{b}_1 + y'\mathbf{b}_2 = \frac{x'}{2}\mathbf{a}_1 + \frac{y'}{2}\mathbf{a}_2$$

where $\mathbf{b}_1$ and $\mathbf{b}_2$ are unit cell vectors of the square lattice, and $\mathbf{a}_1$ and $\mathbf{a}_2$ are the unit cell vectors of the f.c.c. lattice on the projected plane. The corresponding reciprocal lattice vector $\mathbf{k}$ for the square lattice is

$$\mathbf{k}' = 2\pi\left(h'\mathbf{b}_1^* + k'\mathbf{b}_2^*\right) = 2\pi\left(2h'\mathbf{a}_1^* + 2k'\mathbf{a}_2^*\right)$$

where $\mathbf{b}_1^*$ and $\mathbf{b}_2^*$ are corresponding reciprocal unit cell vectors for the square lattice, and $\mathbf{a}_1^*$ and $\mathbf{a}_2^*$ are the reciprocal unit cell vectors for the lattice defined by the real space unit cell vectors, $\mathbf{a}_1$ and $\mathbf{a}_2$.

Therefore, on the projected 2-D square lattice, the kinetic equation in the reciprocal space is given by

$$\frac{d\tilde{P}(\mathbf{k}', t)}{dt} = \frac{c_A(1-c_A)}{k_B T}L(\mathbf{k}')\left\{\tilde{V}(\mathbf{k}')\tilde{P}(\mathbf{k}, t) + k_B T\left[\ln\left(\frac{P(\mathbf{Ar}, t)}{1-P(\mathbf{Ar}, t)}\right)\right]_{\mathbf{k}'}\right\} + \xi(\mathbf{k}', t) \quad (10)$$

with

$$V(\mathbf{k}') = 4W_1(\cos 2\pi h'\cdot\cos 2\pi k' + \cos 2\pi h' + \cos 2\pi k') + 2W_2(\cos 4\pi h' + \cos 4\pi k' + 1) + \cdots \quad (11)$$

and

$$\tilde{L}(\mathbf{k}') = -4L_1[3 - \cos 2\pi h' \cdot \cos 2\pi k' - \cos 2\pi k' - \cos 2\pi h']. \quad (12)$$

3.3. *Generation of thermal noise*

To generate random numbers which satisfy the fluctuation–dissipation theorem, first a random number, μ, is generated at any given lattice point at a given time step from a normal distribution, a Gaussian with average 0.0, and standard deviation 1.0. The random numbers are then multiplied by a factor to obtain the desired variance

$$\xi(\mathbf{r}, t) = p_f \sqrt{\frac{2k_B T L_1 \Delta t}{a_s^2}}\, \mu(\mathbf{r},\mathbf{t}) \quad (13)$$

where Δt is the timestep increment, a_s is the lattice parameter of the square lattice and L_1 is the exchange probability defined earlier. The coefficient, p_f, is a constant which is introduced as a correction factor that takes into account the fact that the correlation equations have been derived from linearized kinetic equations which are valid only at infinitely high temperatures, and the current simulations are being performed using a non-linear kinetic equation at finite temperatures [17, 18]. It serves to ensure that the noise term does not become too large, and is chosen such that numerical stability is maintained.

3.4. *Numerical solution to the kinetic equations*

For many cases, in particular for those involving long-range interactions, it is desirable to solve the kinetic equations in the reciprocal space [19]. Thus, the numerical simulation procedure consists of (1) generating the initial single-site probability distribution, $P(\mathbf{Ar},0)$; (2) calculating $\tilde{L}(\mathbf{k})$ and $\tilde{V}(\mathbf{k})$ from atomic mobilities and interatomic interactions; (3) computing $\mathrm{d}\tilde{P}(\mathbf{Ak}, t)/\mathrm{d}t$ from equation (7); (4) integrating the kinetic equation using the explicit Euler's method; and (5) Fourier transforming $\tilde{P}(\mathbf{Ak}, t)$ back into real space to produce the single-site occupation probability for each site as a function of time, and thus the kinetics of atomic ordering and compositional clustering, as well as the morphological evolution.

4. RESULTS

In this paper, a two-neighbor interaction model is assumed for the Al–Li system and the values for the interaction parameters W_1 and W_2 were calculated from the $V(0)$ and $V(\mathbf{k}_0)$ values reported by Schmitz and Haasen [20], as 40.44 meV/atom and -31.59 meV/atom, respectively. The variation in the interatomic interaction parameters with composition was ignored. The low-temperature part of the $\alpha + \delta'$ two-phase field using these interaction parameters is reproduced in Fig. 1(a), in which the dot-dashed line (T_-) represents the ordering instability line below which a disordered phase is absolutely unstable with respect to ordering, the thin solid line (T_0) is the locus along which the ordered and disordered phases have the same free energy, the dashed line (T_+) is the disordering instability line above which an ordered phase is absolutely unstable with respect to disordering, and the thick solid lines are equilibrium phase boundaries. The free energy curves for the ordered and disordered phases as a function of composition at $T = 465$ K are shown in Fig. 1(b). According to Fig. 1(a) and (b), at this temperature the equilibrium composition (of Li in atomic or mole fraction) of the disordered phase (α), c_α, is ~ 0.068; the equilibrium composition of the metastable ordered phase δ', $c_{\delta'}$, is ~ 0.224; the composition at which the disordered phase becomes absolutely unstable with resect to δ' ordering, or the instability composition, c_-, is ~ 0.131; the composition at which the δ' ordered phase is absolutely unstable with respect to disordering, c_+, is $\sim 0.1.6$; and the composition at which the ordered and disordered phases have the same free energy, c', is ~ 0.109. Computer simulations were performed for several representative compositions within the $\alpha + \delta'$ two-phase field, namely 0.078, 0.10, 0.12, and 0.15 at $T = 465$ K. In all simulations, the initial condition for the single-site occupation probability function corresponds to the completely disordered phase, which was obtained by assigning the occupation probability at each site equal to the average composition. All employed supercells consisting of 64×64 unit cells on the projected 2-D square lattice. Periodic boundary conditions are applied.

4.1. *c = 0.15*

For this composition, the timestep size was 0.005, and the simulations were run for 40,000 timesteps, without thermal noise. The temporal evolution of the atomic configurations and the development of a two-phase morphology are shown in Fig. 2 at different timesteps. The occupational probability of Al is represented by a gray scale on which black indicates 0 and white 1.0. Since the alloy with composition $c = 0.15$ at $T = 465$ K lies below the ordering instability line, it is expected, that the disordered phase will initially undergo a congruent, spinodal ordering process, followed by spinodal decomposition. It can be seen from Fig. 2 that the initially disordered matrix undergoes a spinodal ordering reaction, throughout the system, producing a single-phase $L1_2$ ordered microstructure, with the order domains being separated by antiphase domain boundaries (APBs). In this transient ordered single phase, Al and Li atoms arrange themselves in a fashion consistent with an $L1_2$ projection. A check on the local composition of Li within the ordered domains in this ordered single phase shows it to be very close to 0.15 except at the antiphase domain boundaries around which some compositional redis-

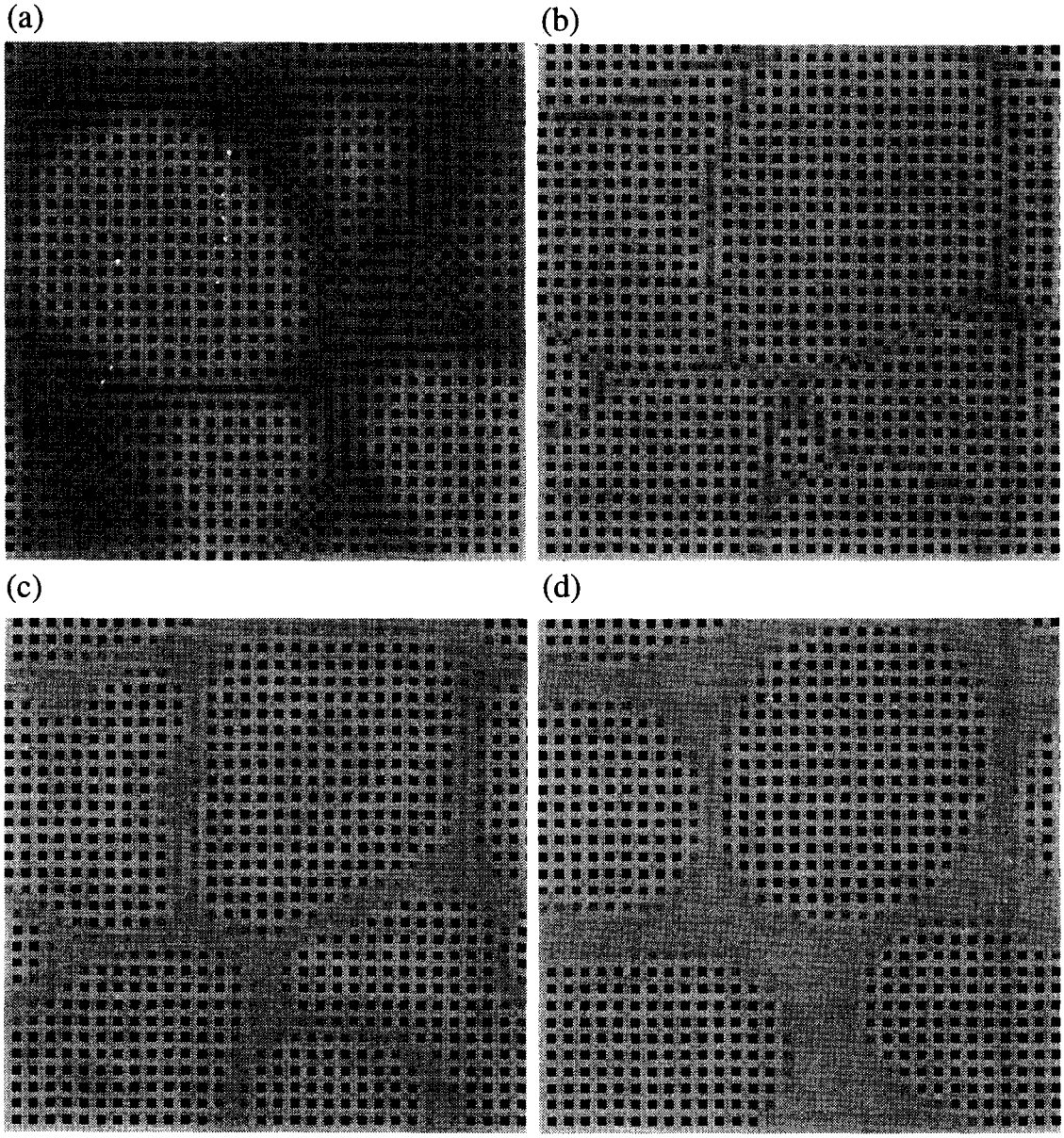

Fig. 2. Computed microstructures for $c_{Li} = 0.15$, at different times t: (a) $t = 10.2$, (b) $t = 12.00$, (c) $t = 30.00$ and (d) $t = 240.00$.

tribution took place accompanying the ordering process, which confirms the fact that the ordering is essentially congruent.

Once congruent ordering has taken place, the disordered phase begins to grow, primarily at the APBs. It is clear from Fig. 2 that simultaneously with the growth of the disordered phase from the APBs, the ordered regions begin to separate into solute-rich and solute-lean regions, exactly as predicted by the phase diagram. The solute-lean regions finally reach a composition which is below c_+, and undergo a spontaneous disordering reaction. Clearly, however, the growth of the disordered phase is much faster at the APBs than within the ordered domains [19]. Thereafter, coarsening sets in, and the disordered phase that is locked within an ordered domain begins to disappear. Also, smaller domains begin to disappear, to be replaced by larger domains.

That congruent ordering precedes compositional decomposition is also proved by Fig. 3, where the average absolute value of the long-range order parameter over the whole system as well as the average absolute deviation of the local composition from the overall average composition (0.15) are plotted against time. The fact that the order parameter reaches a high value before the local composition has deviated from the average compo-

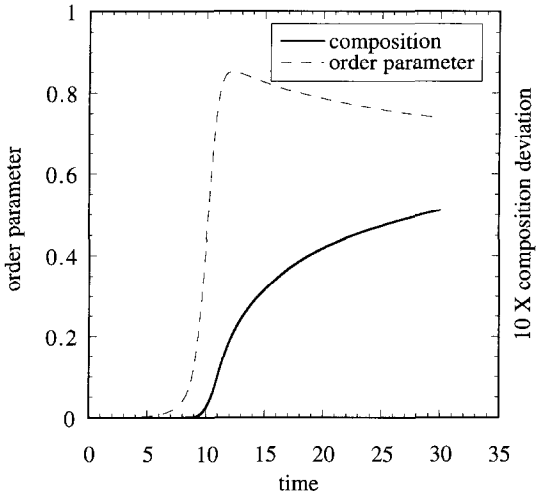

Fig. 3. Variation in order parameter and composition deviation with time, for $c_{Li} = 0.15$.

sition indicates that congruent ordering has indeed taken place first. The local composition as a given lattice site was obtained by averaging over a square of nine lattice sites on the 2-D square lattice. The decrease in the average long-range order parameter after attaining a high value is consistent with the fact that as the disordered phase grows in size, the volume fraction of the ordered phase decreases.

4.2. $c = 0.12$

Figure 4 shows a series of simulated pictures for $c_{Li} = 0.12$, a composition that lies between $c' = 0.109$ and $c_- = 0.131$. The occupation probability of Al is depicted on a gray scale on which black is 0, and white 1.0. Based on the thermodynamic analysis, in this region, the disordered phase is expected to undergo congruent ordering by a nucleation and growth mechanism [1]. Indeed, our simulation showed that random noise introduced to the initial occupation probability distribution decays as simulation proceeds. Therefore, random thermal noise was added to the kinetic equation according to the fluctuation–dissipation theorem for a certain period of time, to promote the nucleation of ordered domains. A nucleus is considered to be critical if it continues to grow when the noise term is switched off and if it disappears when the noise term is switched off one timestep too soon. Once a critical nucleus is identified, the composition and order parameter profiles are analysed. With p_f in expression (13) equal to 0.13 and Δt equal to 0.0002, a critical nucleus was found to form after 22,000 timesteps. After the formation of stable nuclei, the noise term was switched off, Δt was raised to 0.005, and the growth of the ordered domains was followed for another 40,000 timesteps.

It is apparent from Fig. 4, that ordered domains nucleate and grow, until a mixture of two equilibrium phases is reached, but that one does not observe a congruently ordered single-phase microstructure before compositional phase separation. This fact is also shown in Fig. 5, in which the average long-range order parameter and average compositional fluctuation are plotted vs time. The sudden drop in the values of the composition and long-range order parameter before their significant growth is due to the switch-off of noises and due to the fact that the local averaging using only nine lattice points contains artificial contributions from the random noise. The fact that both curves increase at the same time, after the noise term has been switched off, indicates that decomposition and ordering take place simultaneously. This is contrary to what is predicted based on thermodynamics in the composition range [1], but seems to be consistent with our recent prediction using non-classical nucleation theory [12].

The critical composition and order parameter profiles across a critical nucleus are shown in Fig. 6(a) and 6(b). It is quite clear that the critical nucleus contains fluctuations in both composition and long-range order. For comparison, the composition and long-range order profiles obtained from the non-classical nucleation theory are also plotted (filled circles in Fig. 6).

4.3. $c = 0.10$

Compared to a composition of $c = 0.12$, nucleation of an ordered particle at lower compositions is more difficult. In a simulation, it requires an enormously large number of timesteps before a critical nucleus can form. Therefore, in order to speed up the formation of a critical nucleus, we added the same spatial distribution of noise at each timestep for the composition $c = 0.10$. We claim that since our main interest is in the properties of the critical nucleus instead of the nucleation rate, how a critical nucleus is formed is not very important. In fact, our test showed that for a composition of $c = 0.12$, the properties of the critical nucleus obtained by this method are similar to those obtained by thermal noises which are uncorrelated in both space and time [Fig. 7(a) and 7(b)].

Simulations were performed for $c_{Li} = 0.10$, using $p_f = 0.012$ and $\Delta t = 0.005$. The number of timesteps required to form critical nuclei was found to be 1100. Since in this part of the phase diagram the free energy of the disordered phase is lower than that of the ordered phase, it is expected thermodynamically that congruent ordering cannot take place. Indeed our simulation shows a typical nucleation and growth process for the precipitation of ordered particles.

The variation in the local composition and local order parameter across the nucleus, just after it is formed, is plotted in Fig. 8. Both the composition and the order parameter near the center of the critical nucleus are significantly higher than those for the critical nuclei at $c = 0.12$. The corresponding profiles obtained using the continuum equations are also plotted alongside for comparison.

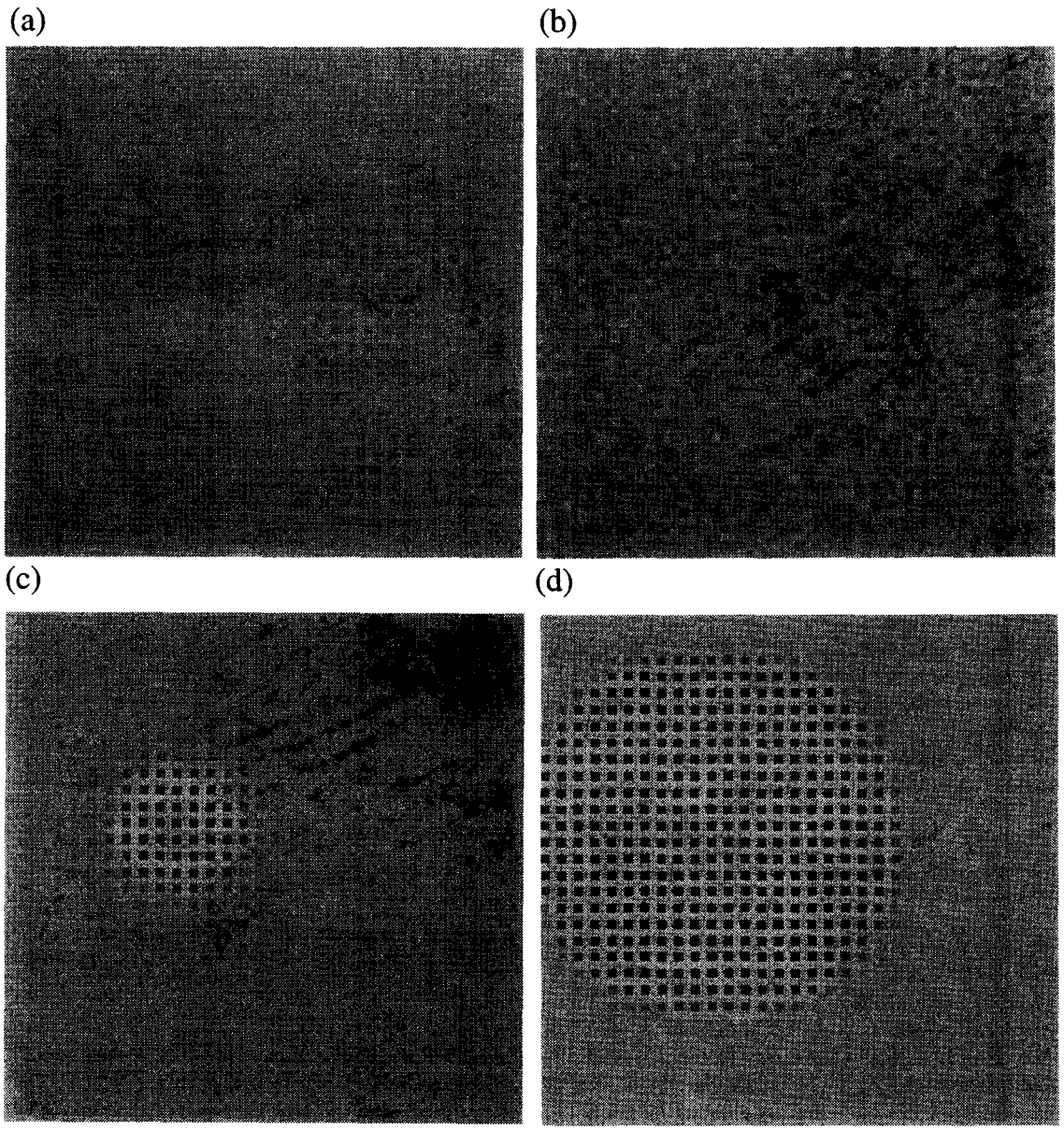

Fig. 4. Computed microstructures for $c_{Li} = 0.12$, at different times t: (a) $t = 4.40$, (b) $t = 5.40$, (c) $t = 14.40$ and (d) $t = 194.40$.

4.4. $c = 0.078$

At this composition also, a stable nucleus forms and grows to an equilibrium size. The noises were generated in the same way as for a composition of $c = 0.10$ with a slightly higher value of $p_f = 0.015$. A critical nucleus was formed after 8600 timesteps. An analysis of the composition and long-range order parameter across the critical nucleus revealed that its composition was higher than the equilibrium phase composition, but then fell back to the equilibrium value at a later time during its growth. This is entirely consistent with the parallel tangent construction for classical nucleation, indicating that classical nucleation theory applies with greater accuracy at this composition than at Li = 0.10 and Li = 0.12. The composition within the nucleus reached at value close to 0.239 and the order parameter value was about 0.98 (see Fig. 8).

5. DISCUSSION

It is clear from the previous results that homogeneous congruent ordering precedes compositional decomposition when a system is below the ordering instability line, such as in the case for a composition of $c = 0.15$. This can be seen not only from the early stage morphologies of ordered domains separated only by APBs, but also from time dependencies of average order parameter and average deviation

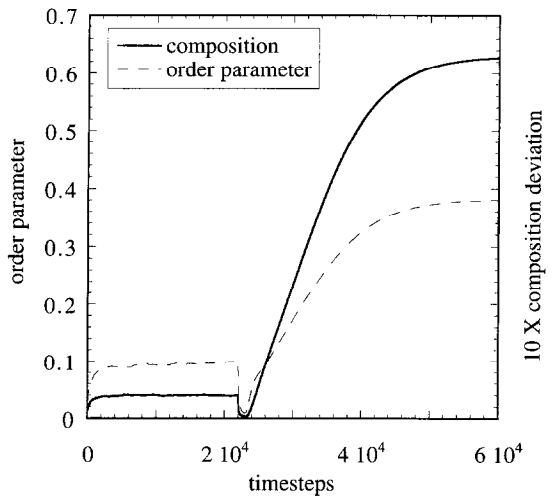

Fig. 5. Variation in order parameter and composition deviation with time, at $c_{Li} = 0.12$.

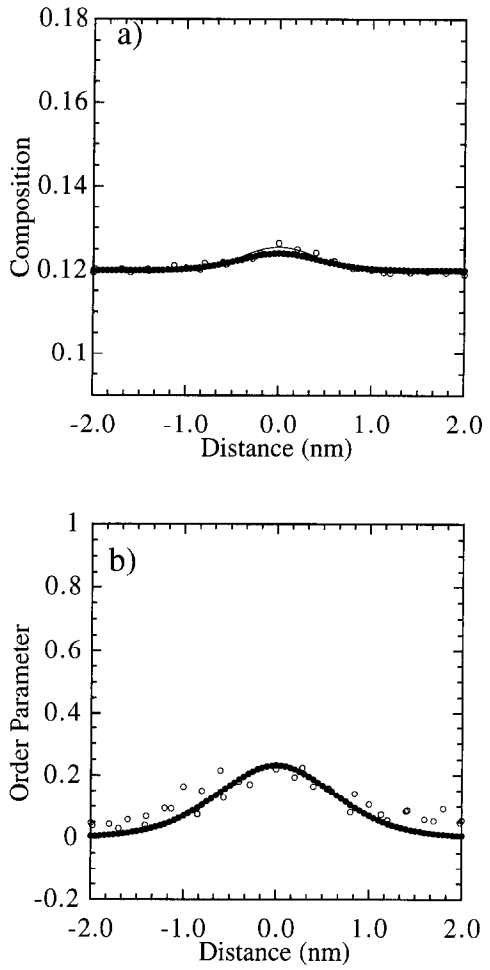

Fig. 6. (a) Composition and (b) order parameter profiles across a critical nucleus for $c_{Li} = 0.12$, using microscopic (open circles) and continuum equations.

from overall composition. The fact that the order parameter reaches a high value before composition fluctuation can take place clearly indicates congruent ordering preceding decomposition.

However, it is important to point out that the time lag between the onset of congruent ordering and the onset of compositional decomposition is extremely short. Therefore, it is not surprising that Hono *et al.* [6] and Schmitz *et al.* [7] could not detect the congruent order stage in their APFIM and HREM studies, respectively. An estimate of the time lag between the two processes may be obtained by noting that the correspondence between real time and the time used in the simulations is approximately given by $t = t^*/L_1$, where L_1 is the inverse of the time it takes for the diffusing species to make a unit jump [19]. This quantity can be estimated using [13] $L_1 \sim D/a_0^2$, where D is the diffusion coefficient at this temperature and a_0 is the lattice parameter. Using $D = 6.47 \times 10^{-15}$ cm^2/s, and $a_0 = 4 \times 10^{-8}$ cm [2, 4], we obtain $L_1 \sim 4.0\ s^{-1}$. Then, the relationship between real time and simulation time is simply $t = 0.25\ t^*$. Since the time lag between the onset of homogeneous congruent ordering the onset of compositional decomposition appears to be only 400 timesteps with a timestep of 0.005 (see Fig. 3), the time lag in terms of the reduced time unit is $t^* = 0.005 \times 400 = 1$ and in terms of the real time lag is 0.25 s. This is clearly too small to be reliably detected by currently available experimental techniques. It is entirely possible that decomposition had already set in even before the quenching process could be completed [7].

Our simulation results also showed that congruent ordering does not take place when $c' < c < c_-$ such as $c = 0.12$, and that ordering and decomposition take place simultaneously through a nucleation and growth process, as demonstrated by the concurrent growth of both the order parameter and the compositional fluctuations. However, a close look at the cross-sections of the critical nuclei reveals that they do not have the properties of the equilibrium ordered phase as assumed by the classical nucleation theory. For example, at $c_{Li} = 0.12$, the composition at the center of a critical nucleus is only slightly higher than 0.12, with an order parameter of only 0.3–0.4. These profiles are nevertheless very similar to those obtained using non-classical nucleation theory in cylindrical coordinates (for the sake of the comparison with the simulation results on the projected plane) (Fig. 6). Also, note that in Fig. 6(a), the critical nucleus composition is such that it is very difficult to make a distinction between "bulk" and "interface". Therefore, the concepts of "bulk" free energy and "interfacial" free energy from classical nucleation theory break down at this composition.

As the average composition of Li is decreased to 0.1 and then to 0.078, the properties of a critical nucleus are increasingly closer to the classical description, i.e. the composition and order parameter values are very close to those of the equilibrium

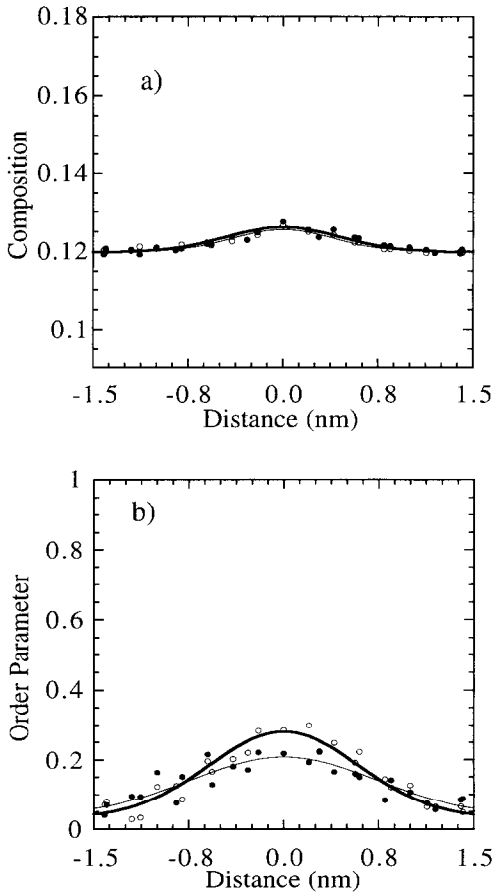

Fig. 7. (a) Composition and (b) order parameter profiles across a critical nucleus for $c_{Li} = 0.12$, using the two different methods of introducing noise.

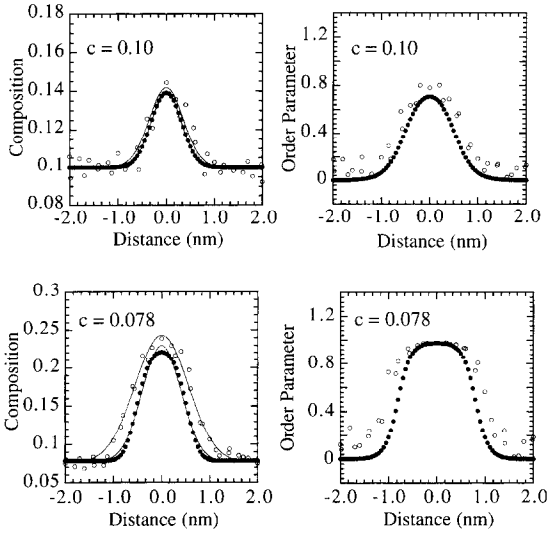

Fig. 8. Composition and order parameter profiles across a critical nucleus for $c_{Li} = 0.10$ and $c_{Li} = 0.078$, using microscopic (open circles) and continuum equations.

ordered phase when the average composition is near the disordered phase boundary. This is consistent with the non-classical nucleation theory of Cahn and Hilliard [21, 22] for isostructural decomposition and our recent work on precipitation of ordered intermetallics [12]. As the average composition approaches the disordered phase boundary, the incipient nucleus composition becomes closer and closer to the equilibrium precipitate composition. The critical nucleus order parameter is mostly constant at the center, and then gradually falls towards its ends. Therefore, it is possible to distinguish between "bulk" and "interface" for this nucleus, although even here the interface is diffused, and not sharp. If l defined as the "thickness" of the interface and r is defined as the radius of the nucleus, then Cahn and Hilliard [21, 22] have stipulated that classical nucleation theory is applicable only when $l \ll r$.

It should be pointed out that the values for p_f in equation (13) were chosen quite arbitrarily to save computational time and to provide numerical stability. We have made no attempt to justify the values theoretically. If our main interest is in the nucleation rate, then the choice of the p_f value will become very important, and has to be justified. As mentioned earlier, our main interest is in the determination of critical composition and long-range order parameter profiles as a function of composition and temperature. Therefore, how a critical nucleus is created is not very crucial and we have shown that the properties of a critical nucleus are very similar even if the ways of generating the noise are very different [Fig. 7(a) and 7(b)].

It is interesting to compare the critical nucleus size obtained from the simulations, with values calculated based on the classical nucleation theory. For calculating the size of a classical nucleus, the interfacial energy is first calculated from a flat boundary between the equilibrium disordered phase and the δ' order phase. Then the driving force for nucleation is estimated by drawing a tangent line to the free energy curve of the disordered phase at the matrix composition, and calculating the largest difference between the free energy curve of the ordered phase and this tangent line. Finally the free energy change for an ordered phase particle is calculated from the interfacial energy and the driving force, by assuming that the particle is cylindrical. The size of the critical nucleus can then be calculated by maximizing the free energy change with respect to the radius of the particle, which gives $r^* = -\sigma/\Delta G_v$, where ΔG_v is the driving force for nucleation (a negative quantity), and σ is the interfacial energy. The nucleus is assumed to be cylindrical for the purpose of comparison with the simulations, where a projection scheme has been employed. These values are plotted in Fig. 9, together with the estimated radii from the non-classical nucleation theory and from the simulation, in which the size is estimated from the half-width of the composition profiles. In Fig. 9, the values for overall composition below the spinodal ordering line indicate the average size of the ordered

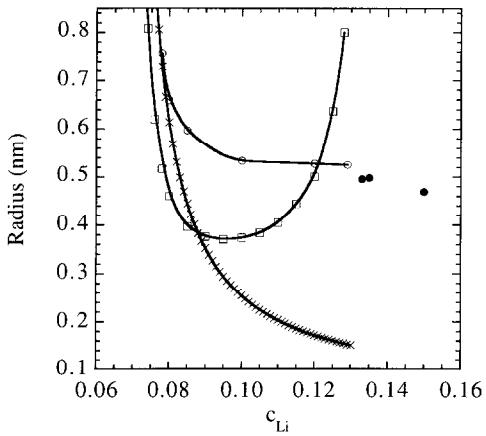

Fig. 9. Critical nucleus radius, using classical nucleation theory (crosses), non-classical nucleation theory (squares) and the current simulations (circles). Filled circles are estimated average sizes of ordered domains in the congruently ordered single phase, for $c > c_-$.

domains when the entire system has just attained the congruent ordering stage.

While the non-classical nucleation theory predicts that there is a divergence in the radius of a critical nucleus as the overall composition approaches the spinodal ordering composition (c_-) (see Fig. 9), our computer simulation with a thermal noise indicates that the domain size is finite both just above and just below the ordering instability line. This is consistent with the results of Binder [23], who postulated that the divergence in the critical nucleus radius near a spinodal line would vanish, if a noise term was added to the Cahn–Hilliard equation. Our computer simulations show that for average compositions below but near the ordering instability line, simulations with a thermal noise added for an extended period of time produce a smaller size of ordered domains than do simulations with only random noise at the initial single-site occupation probability distribution. This means that without the thermal noise term, the size of the ordered domains would diverge just below the spinodal ordering line as well. However, even with thermal noise, congruent ordering does take place and the domain sizes with and without noise are comparable at later times after decomposition.

6. CONCLUSION

A computer study has been performed of the kinetics of the δ' precipitation reaction in Al–Li alloys. It is found that when the Li composition is below the ordering instability line (c_-), precipitation involves congruent ordering followed by decomposition. However, the time lag between the onset of congruent ordering and the onset of compositional decomposition is extremely short (shorter than the incubation time for ordering), making it almost impossible to detect the congruently ordered state experimentally. Below c_-, δ' forms by a nucleation and growth process, the nature of which changes from classical to non-classical nucleation, as the composition increases from the disordered phase boundary. The formation of a critical nucleus cannot be described using only composition fluctuations, as it requires critical fluctuations in both composition and order parameter values. Both composition and long-range order parameter values within the nucleus decrease as the average composition of the system approaches the ordering instability line, but there is no divergence in the size of the critical nucleus, which characterizes the non-classical nucleation mechanism.

Acknowledgements—This work is supported by the Office of Naval Research Young Investigator Program under grant number N-00014-95-1-0577. The work was supported in part by a grant of HPC time from the DoD HPC Center, CEWES, on the C90.

REFERENCES

1. A. G. Khachaturyan, T. F. Lindsey and J. W. Morris, *Metall. Trans.* **19A,** 249 (1988).
2. T. Sato and A. Kamio, *Mater. Trans. Jap. Inst. Metals* **31,** 25 (1990).
3. V. Radmilovic, A. G. Fox and G. Thomas, *Acta metall.* **37,** 2385 (1989).
4. M.-S. Yu and H. H. Chen, Report of the Research Group for Study of Phase Separation in Al–Li Based Alloys, p. 45. Light Metal Educational Foundation, Osaka, Japan (1993).
5. B. J. Shaiu, H. T. Li, H. Y. Lee and H. Chen. *Metall. Trans.* **21A,** 1133 (1990).
6. K. Hono, S. S. Babu, K. Hiraga, R. Okano and T. Sakurai, *Acta metall.* **40,** 3027 (1992).
7. G. Schmitz, K. Hono and P. Haasen, *Act metall.* **42,** 201 (1994).
8. K.-E. Biehl and R. Wagner, *Solid → Solid Phase Transformations* (edited by H. I. Aaronson, D. E. Laughlin and C. M. Wayman), p. 185. TMS-AIME, Warrendale, PA (1982).
9. S. Brenner, M. K. Miller and W. A. Soffa, *Solid → Solid Phase Transformations* (edited by H. I. Aaronson, D. E. Laughlin and C. M. Wayman), p. 191. TMS-AIME, Warrendale, PA (1982).
10. D. Chandra and L. H. Schwartz, *Metall. Trans.* **2,** 511 (1971), as reported in Ref. [9].
11. T. DeNys and P. M. Giehlen, *Metall. Trans.* **2,** 1423 (1971), as reported in Ref. [9].
12. R. Poduri and L.-Q. Chen, submitted to *Acta metall.*
13. A. G. Khachaturyan, *Theory of Structural Transformations in Solids*, p. 129. Wiley, New York (1983).
14. Y. Wang, L.-Q. Chen and A. G. Khachaturyan, *Solid → Solid Phase Transformations* (edited by W. C. Johnson, J. M. Howe, D. E. Laughlin and W. A. Soffa), p. 245. TMS-AIME, Warrendale, PA (1994).
15. Shang Keng Ma, *Modern Theory of Critical Phenomena*. W. A. Benjamin Inc., Reading, MA (1976).
16. H. E. Cook, *Acta metall.* **18,** 197 (1970).
17. A. G. Khachaturyan, Y. Wang and H. Y. Wang, *Mater. Sci. Forum* **155–156,** 345 (1994).
18. (a) A. G. Khachaturyan, private communications; (b) T. M. Rogers, K. R. Elder and R. C. Desai, *Phys. Rev.* **B37,** 9638 (1988).
19. L.-Q. Chen and A. G. Khachaturyan, *Scripta metall.* **25,** 61 (1991).

20. G. Schmitz and P. Haasen, *Acta metall.* **40,** 2209 (1992).
21. H. I. Aaronson and K. C. Russell, *Solid → Solid Phase Transformations* (edited by H. I. Aaronson, D. E. Laughlin and C. M. Wayman), p. 371. TMS-AIME, Warrendale, PA (1982).
22. J. W. Cahn and J. E. Hilliard, *J. Chem. Phys.* **31,** 688 (1958).
23. K. Binder, in *Materials Science and Technology*, Vol. 5; *Phase Transformations in Materials*, (edited by R. W. Cahn, P. Haasen and E. J. Kramer), p. 405. VCH, Winheim (1991).